Article

Cell Reports

Inflammation-Induced Oxidative Stress Mediates Gene Fusion Formation in Prostate Cancer

Graphical Abstract

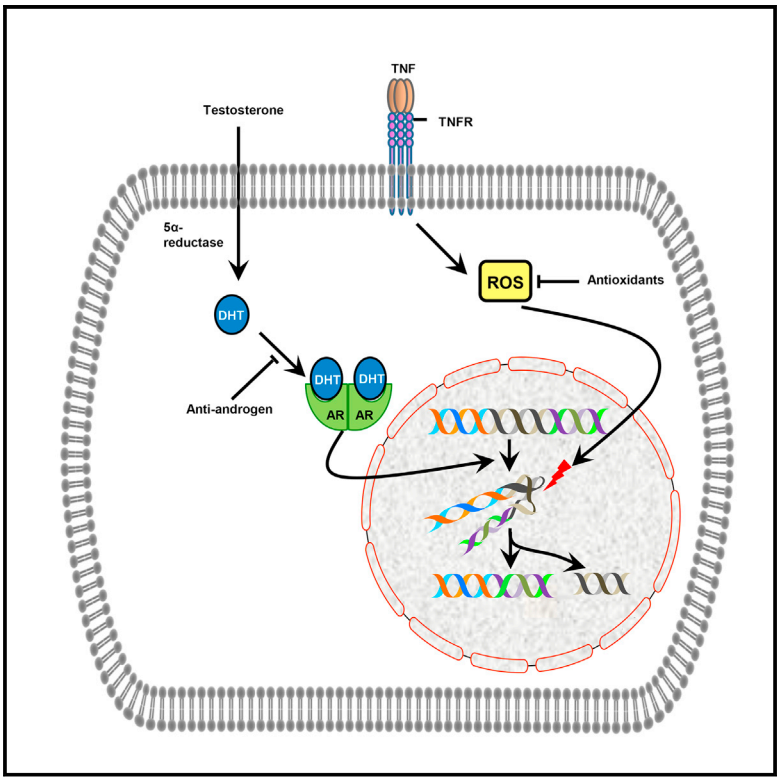

Highlights

- TNF-α induces *TMPRSS2-ERG* gene fusion formation in androgen-responsive cells
- DNA damage by oxidative stress mediates TNF-α-induced gene fusion formation
- Androgen signaling is required for TNF-α-induced *TMPRSS2-ERG* gene fusion formation
- The non-homologous end-joining (NHEJ) pathway is associated with genomic rearrangements

Authors

Ram S. Mani, Mohammad A. Amin, Xiangyi Li, ..., Payal Kapur, Alisa E. Koch, Arul M. Chinnaiyan

Correspondence

ram.mani@utsouthwestern.edu (R.S.M.), arul@umich.edu (A.M.C.)

In Brief

While there is considerable evidence in the literature linking inflammation to the development of prostate cancer, there are few direct links to recurrent driver gene mutations. Mani et al. find a role for inflammation-induced oxidative stress in the formation of DNA breaks leading to recurrent *TMPRSS2-ERG* gene fusions.

Mani et al., 2016, Cell Reports *17*, 2620–2631
December 6, 2016
http://dx.doi.org/10.1016/j.celrep.2016.11.019

OPEN ACCESS
CellPress

Cell Reports
Article

Inflammation-Induced Oxidative Stress Mediates Gene Fusion Formation in Prostate Cancer

Ram S. Mani,[1,2,3,*] Mohammad A. Amin,[4] Xiangyi Li,[1] Shanker Kalyana-Sundaram,[5,6] Brendan A. Veeneman,[5,6,7] Lei Wang,[5,6] Aparna Ghosh,[5,6] Adam Aslam,[1] Susmita G. Ramanand,[1] Bradley J. Rabquer,[4] Wataru Kimura,[8,9] Maxwell Tran,[5,6] Xuhong Cao,[5,10] Sameek Roychowdhury,[11] Saravana M. Dhanasekaran,[5,6] Nallasivam Palanisamy,[12] Hesham A. Sadek,[8] Payal Kapur,[1,2] Alisa E. Koch,[4,13] and Arul M. Chinnaiyan[5,6,7,10,14,15,16,*]

[1]Department of Pathology, UT Southwestern Medical Center, Dallas, TX 75235, USA
[2]Department of Urology, UT Southwestern Medical Center, Dallas, TX 75235, USA
[3]Harold C. Simmons Comprehensive Cancer Center, UT Southwestern Medical Center, Dallas, TX 75235, USA
[4]Department of Internal Medicine, University of Michigan Medical School, Ann Arbor, MI 48109, USA
[5]Michigan Center for Translational Pathology, University of Michigan Medical School, Ann Arbor, MI 48109, USA
[6]Department of Pathology, University of Michigan Medical School, Ann Arbor, MI 48109, USA
[7]Department of Computational Medicine and Bioinformatics, University of Michigan, Ann Arbor, MI 48109, USA
[8]Department of Internal Medicine, UT Southwestern Medical Center, Dallas, TX 75235, USA
[9]Life Science Center, Tsukuba Advanced Research Alliance, University of Tsukuba, Ibaraki 305-8577, Japan
[10]Howard Hughes Medical Institute, University of Michigan Medical School, Ann Arbor, MI 48109, USA
[11]Department of Internal Medicine, The James Cancer Center, Ohio State University, Columbus, OH 43210, USA
[12]Department of Urology, Henry Ford Health System, Detroit, MI 48202, USA
[13]VA Ann Arbor, Ann Arbor, MI 48105, USA
[14]Comprehensive Cancer Center, University of Michigan Medical School, Ann Arbor, MI 48109, USA
[15]Department of Urology, University of Michigan Medical School, Ann Arbor, MI 48109, USA
[16]Lead Contact
*Correspondence: ram.mani@utsouthwestern.edu (R.S.M.), arul@umich.edu (A.M.C.)
http://dx.doi.org/10.1016/j.celrep.2016.11.019

SUMMARY

Approximately 50% of prostate cancers are associated with gene fusions of the androgen-regulated gene *TMPRSS2* to the oncogenic erythroblast transformation-specific (ETS) transcription factor *ERG*. The three-dimensional proximity of *TMPRSS2* and *ERG* genes, in combination with DNA breaks, facilitates the formation of *TMPRSS2-ERG* gene fusions. However, the origins of DNA breaks that underlie gene fusion formation in prostate cancers are far from clear. We demonstrate a role for inflammation-induced oxidative stress in the formation of DNA breaks leading to recurrent *TMPRSS2-ERG* gene fusions. The transcriptional status and epigenetic features of the target genes influence this effect. Importantly, inflammation-induced de novo genomic rearrangements are blocked by homologous recombination (HR) and promoted by non-homologous end-joining (NHEJ) pathways. In conjunction with the association of proliferative inflammatory atrophy (PIA) with human prostate cancer, our results support a working model in which recurrent genomic rearrangements induced by inflammatory stimuli lead to the development of prostate cancer.

INTRODUCTION

There is considerable evidence for the role of inflammation in the development of several forms of human cancer (Balkwill and Mantovani, 2001; Coussens and Werb, 2002; Grivennikov et al., 2010); however, the mechanistic details are not clear. Prostate cancer in particular has been associated with proliferative inflammatory atrophy (PIA), a putative precursor lesion indicative of an inflammatory etiology (De Marzo et al., 1999, 2007). In terms of recurrent driver mutations, approximately 50% of prostate cancers are associated with gene fusions of the androgen-regulated gene *TMPRSS2* to the oncogenic erythroblast transformation-specific (ETS) transcription factor *ERG* (Tomlins et al., 2005). Androgen signaling induces spatial proximity between the *TMPRSS2* and the *ERG* gene loci, which in combination with gamma irradiation-induced DNA breaks, facilitates the formation of gene fusions (Lin et al., 2009; Mani et al., 2009). That said, the in vivo mechanisms contributing to DNA breaks that underlie the formation of *TMPRSS2-ERG* are far from clear. Here, we explore the hypothesis that inflammation plays a key role in the genesis of prostate cancer by promoting the formation of recurrent gene rearrangements.

RESULTS

Inflammation Induces *TMPRSS2-ERG* Gene Fusion Formation

The cytokine, tumor necrosis factor alpha (TNF-α), plays a central role in orchestrating the inflammatory response (Baud and

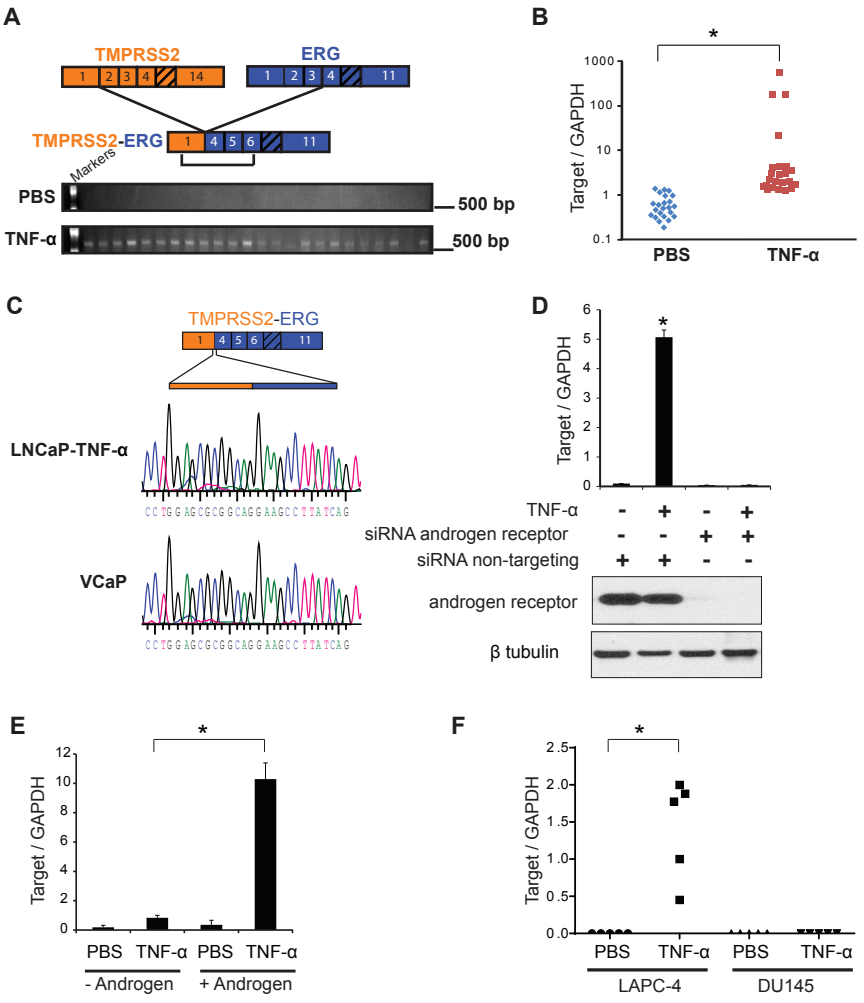

Figure 1. Inflammation Induces *TMPRSS2-ERG* Gene Fusion Formation

(A) Demonstration of *TMPRSS2-ERG* gene fusion transcript formation in LNCaP cells upon stimulation with TNF-α (100 ng/mL) for 48 hr by gel-based RT-PCR analysis. Each treatment is represented by 24 samples.

(B) TaqMan qRT-PCR analysis of the *TMPRSS2-ERG* fusion transcripts in LNCaP cells treated with PBS (n = 23) is compared to TNF-α treatment (100 ng/mL for 48 hr; n = 23; $p < 0.01$ by two-tailed Mann-Whitney U-test). Each data point represents the mean of two technical replicates from an independent treatment.

(C) Sequence analysis of *TMPRSS2-ERG* transcripts in *TMPRSS2-ERG*-positive LNCaP cells obtained by TNF-α stimulation. Gene structures for *TMPRSS2* and *ERG*, respectively, are shown using GenBank: NM_005656 and NM_004449.

(D) Androgen receptor (AR) knockdown blocks TNF-α-mediated *TMPRSS2-ERG* gene fusion formation in LNCaP cells. The top panel represents qRT-PCR analysis of *TMPRSS2-ERG* fusion transcripts (*$p < 0.01$ by two-tailed Student's t test; error bars, SEM of two technical replicates). The bottom panel represents the immunoblot analysis to determine AR knockdown.

(E) qRT-PCR analysis indicates a role for androgens in the formation of *TMPRSS2-ERG* gene fusion transcripts in LNCaP cells (*$p < 0.01$ by two-tailed Student's t test; error bars, SEM of three technical replicates).

(F) Induction of *TMPRSS2-ERG* gene fusion transcripts in the AR-positive cell line, LAPC-4, upon stimulation with TNF-α (100 ng/mL for 48 hr), but not in the AR-negative cell line, DU145. TaqMan qRT-PCR analysis of the *TMPRSS2-ERG* fusion transcript in LAPC-4 or DU145 cells treated with PBS (n = 5) is compared to TNF-α treatment (n = 5; *$p < 0.01$ by two-tailed Mann-Whitney U-test). Each data point represents the mean of two technical replicates from an independent treatment. See also Figure S1.

Karin, 2001). To initially recapitulate the effects of inflammation in vitro, we stimulated the *TMPRSS2-ERG* gene fusion-negative LNCaP prostate cancer cells with TNF-α for 48 hr. To our surprise, we observed robust formation of the *TMPRSS2-ERG* gene fusion transcript by TNF-α stimulation, as assessed by TaqMan-based qRT-PCR and gel-based RT-PCR (Figures 1A and 1B). Gene fusion formation induced by TNF-α was equal to, or more efficient than, exposure to 5 and 50 Gy irradiation (Figure S1A), which we and others have reported on (Haffner et al., 2010; Lin et al., 2009; Mani et al., 2009). This was particularly exciting in that the prostate gland is more likely to be exposed to pro-inflammatory stimuli than to large doses of gamma radiation, making inflammation a more physiologic inducer of gene fusions. The short timescale of these experiments and the observation that stimulation with TNF-α does not increase the levels of *TMPRSS2-ERG* or total *ERG* transcripts in VCaP cells, which endogenously harbor the *TMPRSS2-ERG* gene fusion (Tomlins et al., 2005), indicate that the observed effects are not due to selective growth or survival conferred by the treatment or due to an increase in transcript levels from a fixed population of cells with rearrangements already present (Figure S1B). We therefore report the genesis of gene fusions in the absence of clonal selection. On the basis of standard curve analysis of serially diluted VCaP cells, we estimate the induced *TMPRSS2-ERG* rearrangement frequency in LNCaP cells to be about one event in 10,000 cells (Figure S1C). Sequence analysis of the TNF-α-induced fusion transcripts in LNCaP cells revealed joining of the first exon of *TMPRSS2* with exon 4 of *ERG*, which is the most common *TMPRSS2-ERG* isoform in prostate cancers and is also endogenously present in VCaP prostate cancer cells (Figure 1C) (Tomlins et al., 2005).

We next examined the role of androgen signaling in TNF-α-mediated *TMPRSS2-ERG* gene fusion formation. Depletion of androgens from the media or androgen receptor (AR) knockdown by small interfering RNA (siRNA) blocks *TMPRSS2-ERG* gene fusion formation upon TNF-α stimulation (Figures 1D and 1E). In addition to LNCaP cells, we observe TNF-α-induced *TMPRSS2-ERG* gene fusion formation in LAPC-4

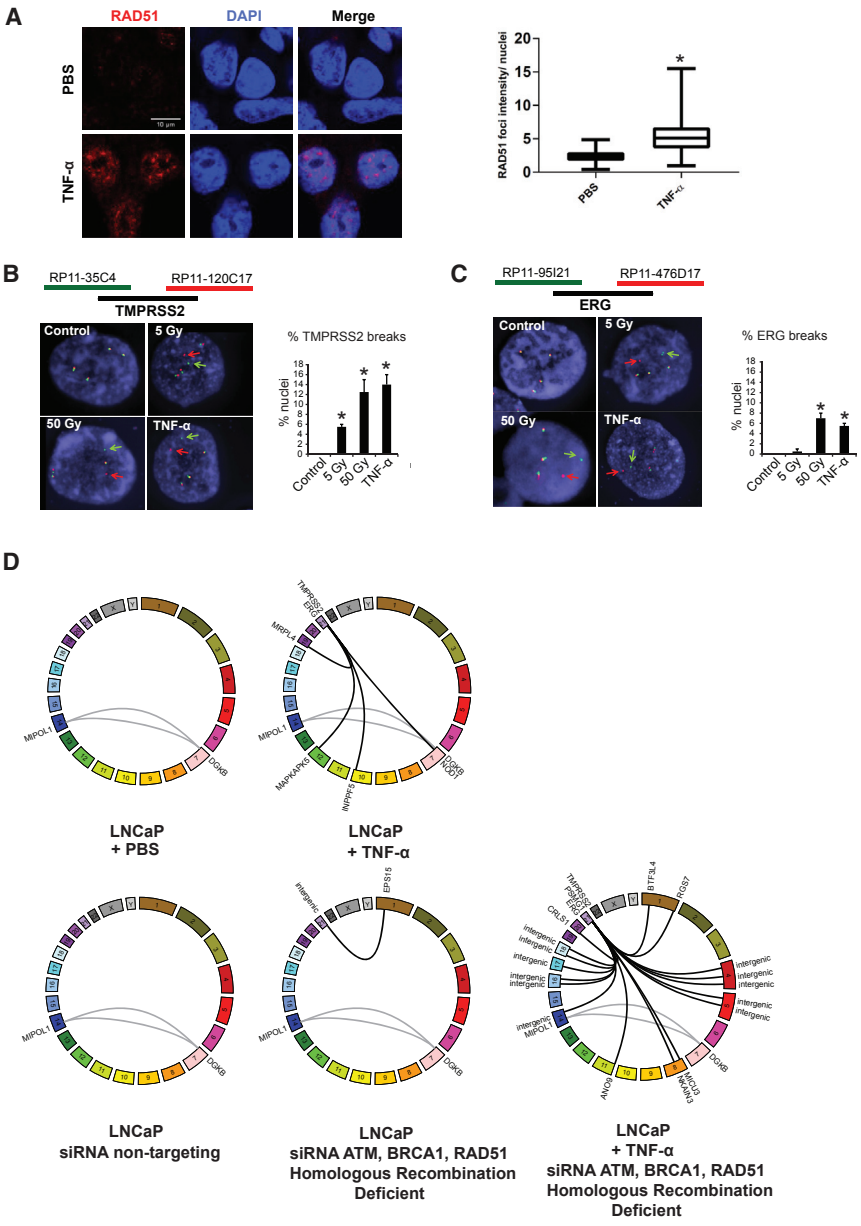

Figure 2. Inflammation Induces De Novo Genomic Rearrangements

(A) RAD51 foci formation upon treatment of LNCaP cells with TNF-α (100 ng/mL). Cells were processed 48 hr post-treatment. Scale bar indicates 10 μm (left). The staining intensity of Rad51 foci was analyzed using the CellProfiler software for 165 nuclei per treatment (*$p < 0.01$ by two-tailed Mann-Whitney U-test) (right).

(B and C) FISH-based detection of DNA breaks at the *TMPRSS2* locus (B) and the *ERG* locus (C). Untreated LNCaP cells are compared to those with TNF-α stimulation (100 ng/mL), 5 Gy gamma irradiation, and 50 Gy gamma irradiation. Cells were processed 48 hr post-treatment. Split signals representing DNA breaks are highlighted by arrows. The FISH images are accompanied by histograms representing the percentage of nuclei with split signals. For *TMPRSS2* and *ERG* loci, 100 nuclei were analyzed per treatment (*$p < 0.05$ by two-tailed Student's t test; error bars, SEM of two technical replicates).

(D) Probe-based custom genomic DNA capture, sequencing, and analysis of LNCaP cells with the indicated treatments. Stimulation with TNF-α induces the formation of de novo chromosomal translocations (top panel). Homologous recombination (HR) deficiency (combined ATM, BRCA1, and RAD51 knockdown) per se is relatively inefficient in inducing chromosomal translocations in the absence of external stress. A combination of TNF-α stimulation and HR deficiency synergistically induces the formation of de novo chromosomal translocations (bottom panel). Genomic rearrangement breakpoints were called from the capture sequencing data and are presented here, grouped by treatment and plotted with Circos. See also Figures S2–S5.

cells that are androgen sensitive. However, the androgen-insensitive DU145 cells are resistant to TNF-α-induced gene fusion formation (Figures 1F and S1D). Stimulation of LNCaP cells with TNF-α does not result in detectable levels of *TMPRSS2-ETV1* gene fusion or *BCR-ABL1* gene fusion, products of inter-chromosomal rearrangement observed in <5% of prostate cancers (Tomlins et al., 2007) or in most chronic myelogenous leukemia (CML) cases (Rowley, 1973) respectively (Figure S1E). Collectively, these results indicate that (1) genomic rearrangements are non-random, cell-type-specific events dictated by lineage-restricted cell signaling pathways (e.g., androgen signaling in prostate cancer), and (2) intra-chromosomal rearrangements (e.g., *TMPRSS2-ERG*) are more prevalent than inter-chromosomal rearrangements.

Inflammation Induces DNA Double-Strand Breaks and De Novo Genomic Rearrangements

To demonstrate that DNA damage occurs upon exposure of LNCaP cells to TNF-α, we monitored phosphorylated histone H2A.X (Ser139), which was elevated within 12 hr of exposure (Figure S2A) and was recruited to known translocation sites at *TMPRSS2* and *ERG* loci (Figure S2B). Stimulation of LNCaP with TNF-α resulted in RAD51 foci formation, indicating initiation of DNA repair function (Figure 2A). Furthermore, by employing a split-signal-based dual-color fluorescence in situ hybridization (FISH) assay, we observed breaks in the *TMPRSS2* and *ERG* loci upon stimulation of LNCaP cells with TNF-α (Figures 2B and 2C). Gamma radiation (5 and 50 Gy), as previously shown (Lin et al., 2009; Mani et al., 2009), induced breaks in these loci and was included as a positive control. We observed that *TMPRSS2* is more prone to DNA breaks in comparison to *ERG*. Because *TMPRSS2* is transcriptionally active before the formation of gene fusions, and *ERG* is not, we speculate that the frequency of DNA breaks at a locus is correlated with its transcriptional activity.

We developed a custom capture sequencing pipeline to study inflammation-induced de novo genomic rearrangements at the single-molecule level in the absence of clonal selection. We designed probes to capture *TMPRSS2*, *ERG*, and a few control loci (e.g., *MIPOL1* and *DGKB*), followed by deep sequencing (>2,000× depth) and analysis. To benchmark our analysis pipeline, we characterized the genomic breakpoints associated with *MIPOL1-DGKB* gene fusion, a clonal rearrangement in LNCaP cells, characterized by two cryptic insertions of a minimal region around *ETV1* (chromosome 7) into the *MIPOL1* gene (chromosome 14) (Maher et al., 2009; Tomlins et al., 2007). We rediscovered the known genomic breakpoint between *MIPOL1* and *DGKB* and also identified a novel second genomic breakpoint between the two genes (Figure S3A). Both breakpoints are associated with junction microhomologies of four and two nucleotides, respectively (Figure S3B).

Next, we de-convoluted the genomic rearrangements associated with *TMPRSS2-ERG* gene fusion in VCaP cells. We rediscovered the four reported breakpoints (Teles Alves et al., 2013; Weier et al., 2013), including an inter-chromosomal rearrangement (Figures S3C and S3D). Two of the four breakpoints exhibited blunt junctions; the remaining two breakpoints displayed, respectively, a single nucleotide junction microhomology and an eight-nucleotide "non-templated" insertion that could not be aligned to either of the contributing loci (Figure S3E). Sanger sequencing analysis confirmed a complex genomic rearrangement involving the sense strand of *TMPRSS2* intron 1, the antisense strand of *TMPRSS2* intron 5, and the sense strand of *ERG* intron 3 as the genomic event contributing to the *TMPRSS2-ERG* gene fusion (Figure S4).

We applied this analysis pipeline to study LNCaP cells treated with PBS or TNF-α. We observed robust formation of de novo genomic rearrangements upon TNF-α stimulation (Figure 2D). Because the short experimental time frame precludes clonal selection, all discovered rearrangements represent single-molecule events. Our stringent algorithm selected only those rearrangements that were supported by junction spanning reads, thereby facilitating detailed analysis of junction characteristics and repair mechanisms.

Because homologous recombination (HR) has been suggested to maintain genome integrity by blocking genomic rearrangements (Moynahan and Jasin, 2010), we tested the effect of a defective HR by simultaneous knockdown of ATM, BRCA1, and RAD51, key players in the HR pathway (Figure S5). Due to the functional redundancy among the major HR players, we hypothesized that silencing multiple HR components will significantly inhibit the HR pathway. We observed that a defective HR, in the absence of an external stress, is relatively inefficient in the formation of genomic rearrangements. A combination of TNF-α stimulation and HR deficiency further increased the formation of de novo genomic rearrangements (Figure 2D). The generally low frequency of the specific genomic rearrangement between *TMPRSS2* and *ERG* genes, due to the absence of clonal selection, precluded us from identifying DNA rearrangement junctions between these two genes. Hence, we focused on identifying the general principles underlying TNF-α-induced DNA rearrangements involving *TMPRSS2* or *ERG* rather than DNA rearrangements between *TMPRSS2* and *ERG* genes.

DNA Sequence and Epigenetic Features of TNF-α-Induced De Novo Genomic Rearrangements

About 75% (19/25) of the induced de novo genomic rearrangement breakpoints exhibit junction microhomology ranging from one to six nucleotides (Figures 3A–3F and S6A). The observed breakpoints exhibited an average microhomology length of 1.84 bp, significantly longer than the average length obtained from 10,000 simulated sets of randomly generated breakpoints ($p < 0.0001$) (Figure 3G). Two of the six blunt junctions exhibit microhomology on the reverse strand, a previously undescribed phenomenon. We speculate that reverse microhomology may facilitate genomic rearrangements by a mechanism involving transient base pairing (Figure S6B). The de novo DNA rearrangements induced by inflammation have characteristics observed in cancer-associated translocations, because a study reported 1 to 4 bp microhomology in most translocation junctions in prostate cancer specimens (Weier et al., 2013). Altogether, these characteristics of the induced breakpoint junctions implicate microhomology-mediated non-homologous end-joining (NHEJ) as the pathway associated with de novo genomic rearrangements.

The recurrently fused intron 3 of *ERG* is 130 kb long and is one of the largest introns in the human genome (Figure 3H). We hypothesized that the DNA sequence and epigenetic features afforded by the large intron size could dictate the formation of TNF-α-induced breaks in a transcription-independent manner. We queried the induced de novo breakpoints against DNA sequence features like non-B DNA structures (inverted repeats, mirror repeats, direct repeats, G-quadruplex-forming repeats, Z-DNA repeats, A-phased repeats, and short tandem repeats). None of these features demonstrated significant enrichment near the observed breakpoints. Upon ruling out DNA sequence elements, we analyzed epigenetic features by querying datasets generated by the Encyclopedia of DNA Elements (ENCODE) project (Consortium et al., 2012; Thurman et al., 2012). A significant fraction of the genomic breakpoints identified in *ERG* lay within DNase I hypersensitivity sites (DHSs) (43.75%, $p < 0.0001$); the genomic breakpoints in *TMPRSS2* were not significantly enriched in DHSs (Figure 3I). This result suggests that DNase I hypersensitivity, and by extension open chromatin, may contribute to the formation of some genomic breaks in *ERG*. We conclude that breaks in *TMPRSS2* are dictated by its transcriptional status and breaks in *ERG* by epigenetic features like DHSs.

Oxidative Stress as the Mediator of Inflammation-Induced Gene Fusion Formation

TNF-α stimulation has been reported to increase reactive oxygen species (ROS) production via multiple mechanisms (Blaser et al., 2016; Chandel et al., 2001; Kim et al., 2007, 2010; Yazdanpanah et al., 2009). We hypothesized that oxidative stress-mediated DNA damage may be the underlying mechanism for the generation of DNA double-strand breaks required for gene fusion formation. Stimulation of LNCaP cells with TNF-α resulted in a dose-dependent increase in ROS production (Figure 4A). Consistent with earlier studies (Kim et al., 2010), we observed that treatment with cycloheximide (CHX), an inhibitor of protein biosynthesis, enhanced TNF-α-induced ROS production (Figure 4A). This is presumably due to CHX-induced blockade of

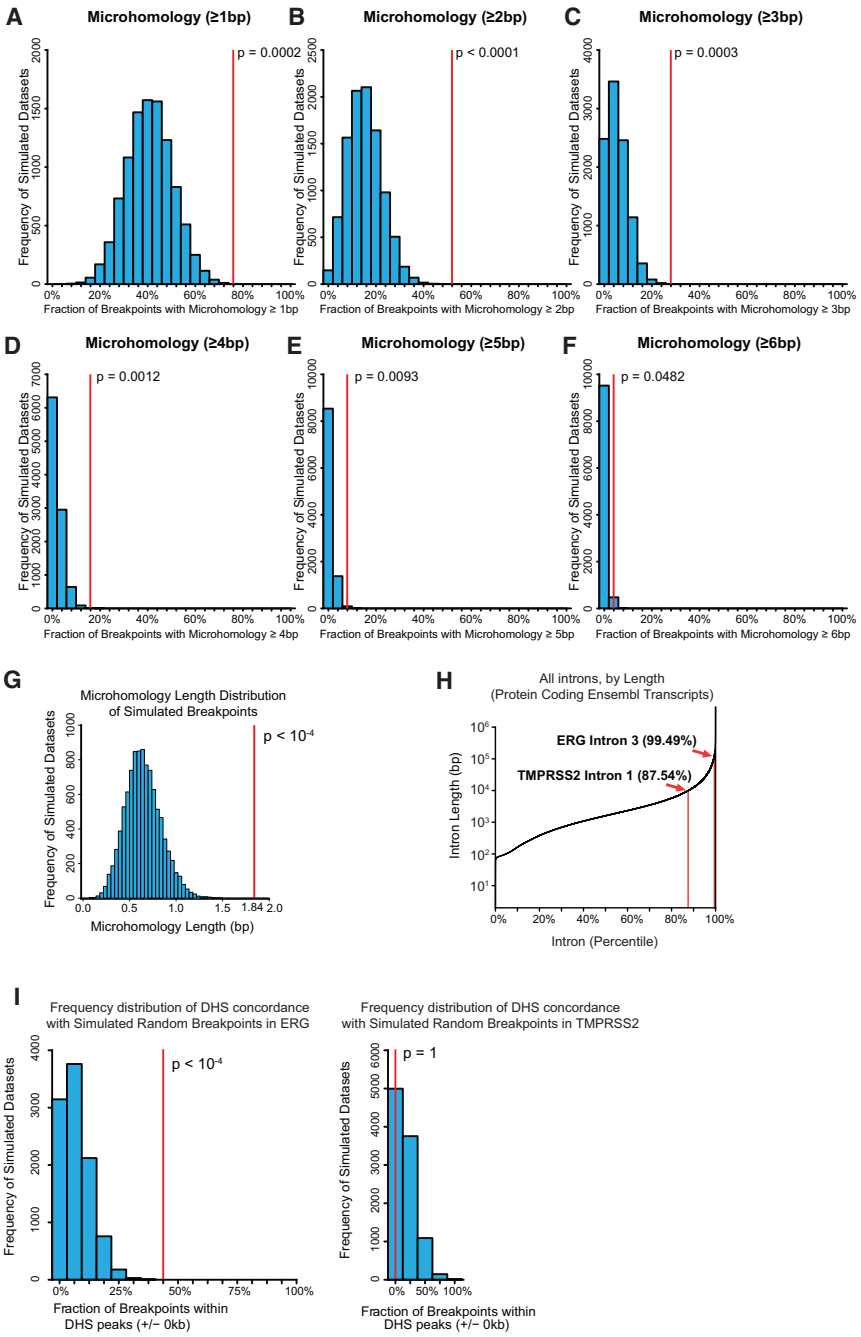

Figure 3. DNA Sequence and Epigenetic Features of TNF-α-Induced De Novo Genomic Rearrangements

(A–F) TNF-α-induced de novo chromosomal translocations are associated with junction microhomologies. The 25 observed genomic breakpoints were compared with distributions of randomly simulated breakpoints (10,000 sets of 25 breakpoints) for six measures of junction microhomology. A significantly greater fraction of the observed breakpoints exhibited junction microhomology than expected by chance, for any length up to six bases. Of the observed breaks, 76% have 1 bp or more of junction microhomology ($p = 0.0002$) (A), 52% have 2 bp or more ($p = 0.0001$) (B), 28% have 3 bp or more ($p = 0.0003$) (C), 16% have 4 bp or more ($p = 0.0012$) (D), 8% have 5 bp or more ($p = 0.0093$) (E), and 4% have 6 bp or more ($p = 0.0482$) (F).

(G) The 25 observed genomic breakpoints were compared with distributions of randomly simulated breakpoints (10,000 sets of 25 breakpoints) for junction microhomology length. The observed breakpoints exhibited an average microhomology length of 1.84 bp, significantly longer than expected by chance ($p < 0.0001$).

(H) *ERG*'s recurrently fused intron is among the largest in the genome. Protein-coding genes in chromosomes 1–22, X, and Y were selected from the Ensembl gene reference, and the longest transcript was taken as representative of each gene. Intron sizes were interpolated from transcript exon boundaries and then sorted and plotted as shown. *ERG*'s recurrently fused intron is 130,040 bases long and is thus larger than 99.49% of annotated introns. *TMPRSS2*'s recurrently fused intron is 9,891 bases long and is thus larger than 87.54% of annotated introns.

(I) Association between *ERG* genomic breakpoints and DNase I hypersensitivity sites (DHSs). DHS peak data were acquired from the ENCODE data portal and filtered for sites identified in greater than 10% of the 125 cell lines profiled. The observed induced genomic breakpoints within *ERG* and *TMPRSS2* were then compared with distributions of randomly simulated breakpoints (10,000 sets of 16 and 10,000 sets of 4). A significantly greater fraction of the genomic breakpoints identified in *ERG* lay within DHSs than expected from the random distribution (43.75%; $p < 0.0001$) (left). The genomic breakpoints in *TMPRSS2* were not significantly enriched in DHSs (right).

See also Figure S6.

nuclear factor κB (NF-κB)-mediated antioxidant production. TNF-α-induced ROS production can be reversed upon treatment with the ROS scavenger N-acetylcysteine (NAC) (Figure 4A). TNF-α-induced ROS production and DNA damage were also observed in the androgen-sensitive LAPC-4 cells, androgen-insensitive DU145 cells, and benign immortalized non-transformed RWPE-1 cells (Figures 4B and 4C). Thus, we conclude that androgen signaling is not required for TNF-α-mediated formation of DNA breaks. Rather, AR redirects ROS-mediated DNA damage to the TMPRSS2 locus by enhancing transcription, opening up the DNA, and thereby making it susceptible to DNA double-strand breaks. TNF-α-induced DNA breaks in the *ERG* locus are likely to be AR independent. This set the stage for the next set of experiments to test the role of oxidative stress in gene fusion formation.

The Role of ROS in ETS Gene Fusion Formation

Although single-agent treatment of LNCaP cells with either TNF-α or CHX induced DNA damage, a combination of TNF-α and CHX markedly enhanced the extent of the DNA damage, as visualized

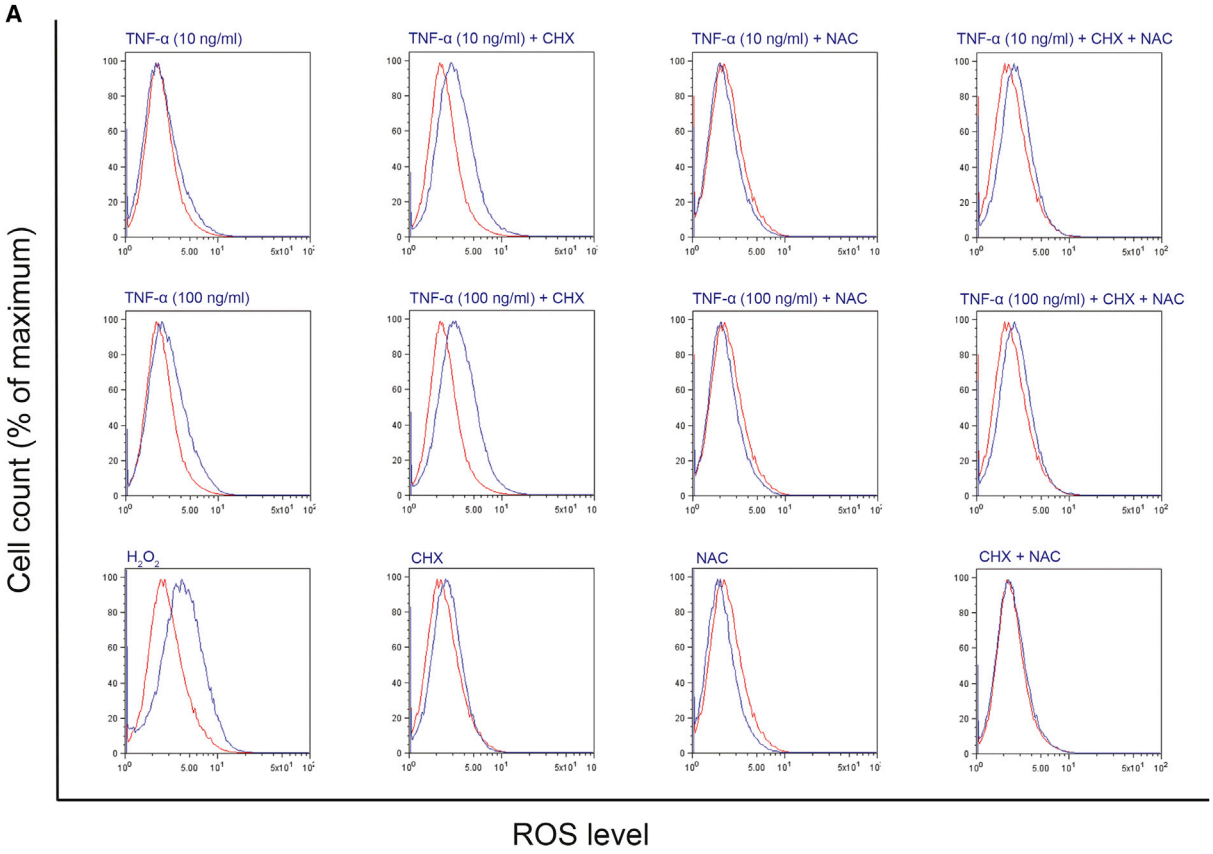

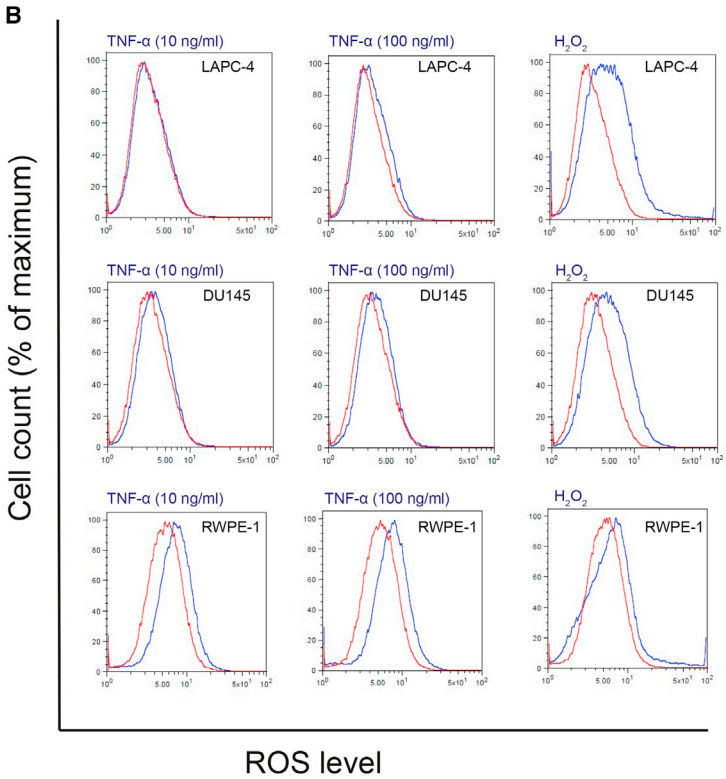

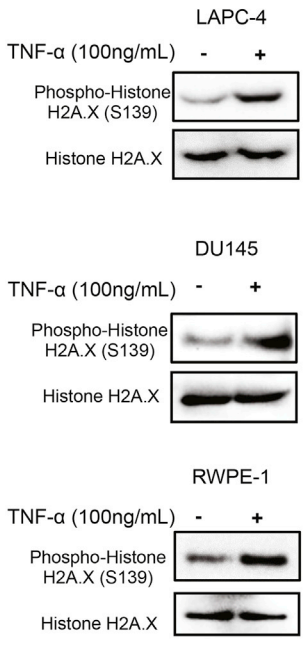

(legend on next page)

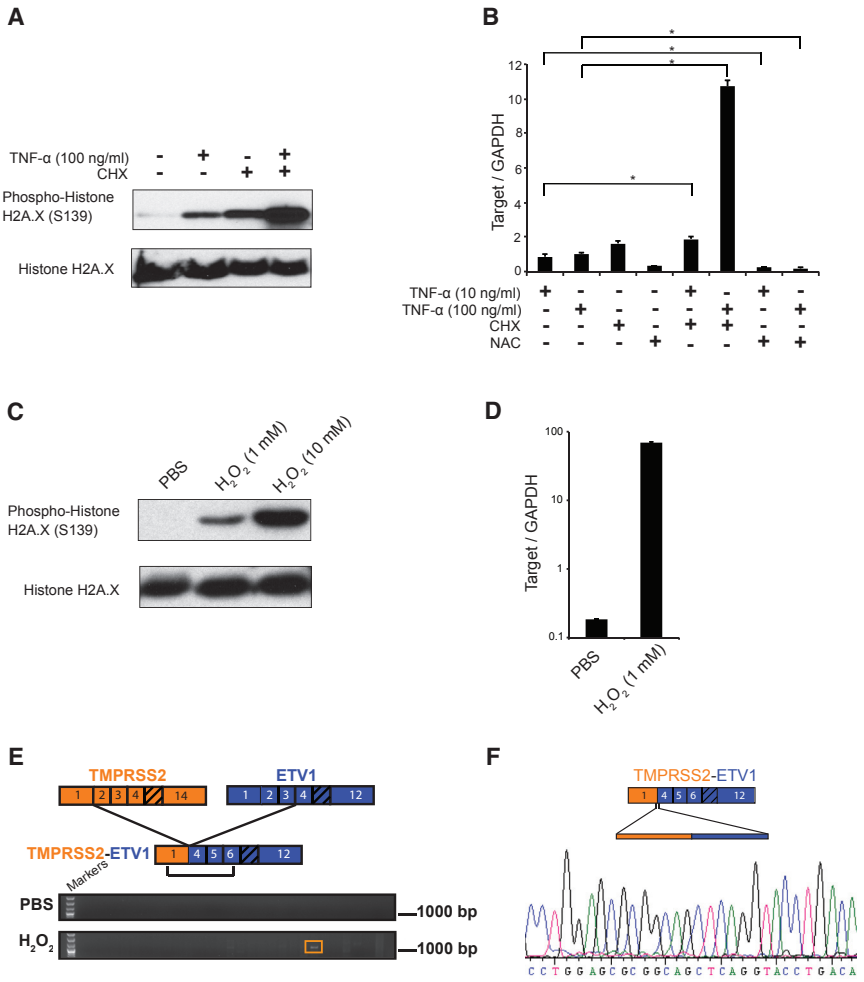

Figure 5. Oxidative Stress Induces *TMPRSS2-ERG* and *TMPRSS2-ETV1* Gene Fusion Formation

(A) Immunoblot analysis of lysates from LNCaP cells stimulated with TNF-α (100 ng/mL), CHX (10 μg/mL), or a combination of TNF-α and CHX for 24 hr are shown with antibodies against phosphorylated histone H2A.X (Ser139) (top) and total histone H2A.X (bottom).

(B) qRT-PCR analysis of *TMPRSS2-ERG* fusion transcripts from LNCaP cells with the indicated treatments for 48 hr (*$p < 0.05$ by two-tailed Student's t test; error bars, SEM of two technical replicates).

(C) Immunoblot analysis of lysates from LNCaP cells stimulated with the indicated doses of H_2O_2 for 24 hr are shown with antibodies against phosphorylated histone H2A.X (Ser139) (top) and total histone H2A.X (bottom).

(D) qRT-PCR analysis of *TMPRSS2-ERG* fusion transcripts from LNCaP cells with the indicated dose of H_2O_2 treatment for 48 hr (*$p < 0.01$ by two-tailed Student's t test; error bars, SEM of two technical replicates).

(E) Demonstration of *TMPRSS2-ETV1* gene fusion transcript formation in LNCaP cells upon stimulation with H_2O_2 (1 mM for 48 hr) by gel-based RT-PCR analysis. The box highlights a band representing *TMPRSS2-ETV1* transcript.

(F) Sequence analysis of *TMPRSS2-ETV1* transcripts in *TMPRSS2-ETV1*-positive LNCaP cells obtained by H_2O_2 stimulation. Gene structures for TMPRSS2 and ETV1, respectively, are shown using GenBank: NM_005656 and NM_004956.

See also Figure S7.

by phosphorylated histone H2A.X (Ser139) western blotting (Figure 5A). Consistent with this observation, the combination of TNF-α and CHX significantly increased *TMPRSS2-ERG* gene fusion formation in comparison to single-agent treatments (Figure 5B). TNF-α-induced *TMPRSS2-ERG* formation was blocked by treatment with NAC (Figure 5B). Thus, ROS is the mediator of TNF-α-induced *TMPRSS2-ERG* gene fusion formation. To recapitulate the effect of TNF-α-induced ROS formation, we treated LNCaP cells with H_2O_2. Treatment with H_2O_2 resulted in a dose-dependent increase in DNA breaks and *TMPRSS2-ERG* gene fusion formation (Figures 5C and 5D). The induction of *TMPRSS2-ERG* gene fusion with H_2O_2 was orders of magnitude higher than stimulation with TNF-α alone. H_2O_2 treatment also induced the formation of the inter-chromosomal *TMPRSS2-ETV1* rearrangement, although the frequency was very low (Figures 5E and 5F). However, we did not observe H_2O_2-induced formation *BCR-ABL1* rearrangement in LNCaP cells, although *BCR* and *ABL1* genes are expressed in these cells (Figure S7A). These results provide further support to the conclusion that gene fusions originate in a non-random, cell-type-dependent manner.

Air-Pouch Model of Inflammation to Study Gene Fusions

Next, we explored whether gene fusions can be induced by inflammation in an in vivo setting. To do this, we took advantage of a well-studied murine model of in vivo inflammation, which occurs in an artificial air pouch (Edwards et al., 1981). The air pouch

Figure 4. TNF-α Stimulation and Intracellular ROS Level

(A) Analysis of ROS formation in LNCaP cells by flow cytometry. The blue and red plots represent treatment and matched controls, respectively. The X axis and Y axis represent ROS level and cell count, respectively, for all plots. TNF-α doses are as indicated. 10 mM N-acetylcysteine (NAC) and 10 μg/mL cycloheximide (CHX) were used in the study. All plots represent 24 hr treatment, with the exception of H_2O_2, a positive control used in the study (3.5 hr treatment) (bottom left).

(B) Analysis of TNF-α-induced (24 hr treatment) ROS formation in LAPC-4, DU145, and RWPE-1 cells.

(C) Immunoblot analysis of lysates from LAPC-4, DU145, and RWPE-1 cells stimulated with TNF-α (100 ng/mL) for 24 hr are shown with antibodies against phosphorylated histone H2A.X (Ser139) (top), and total histone H2A.X (bottom).

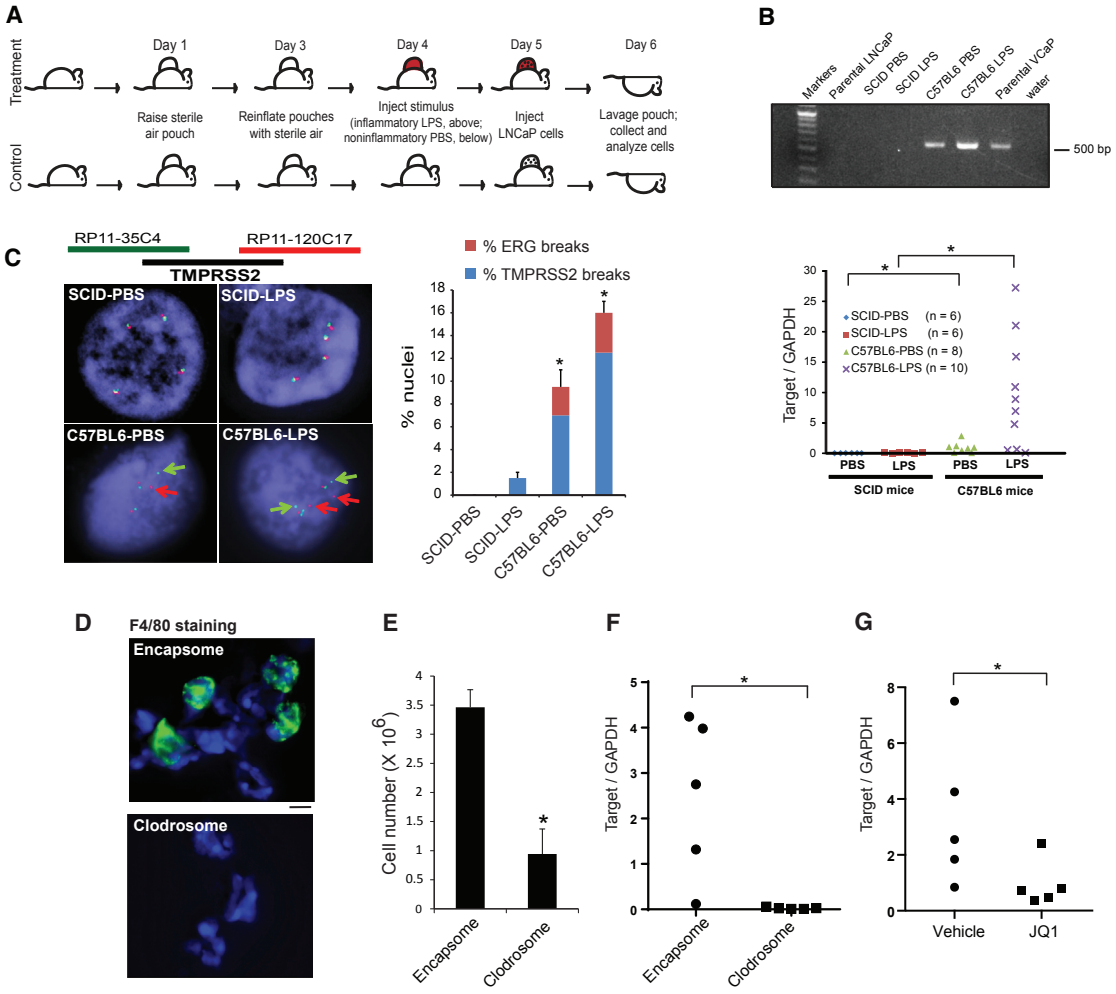

Figure 6. Inflammation Induces In Vivo Gene Fusion Formation

(A) Schematic representation of mouse air-pouch experiments.

(B) TaqMan qRT-PCR assays to determine *TMPRSS2-ERG* transcript level on cells derived from SCID or C57BL/6 mouse air pouches with indicated treatments (*$p < 0.01$ by two-tailed Mann-Whitney U-test) (bottom). Each data point represents the mean of three technical replicates from an independent treatment. Gel-based RT-PCR analysis with primers spanning the first exon of *TMPRSS2* and the sixth exon of *ERG* for representative samples (top).

(C) FISH analysis to detect *TMPRSS2* locus DNA breaks in LNCaP cells derived from C57BL/6 or SCID mouse air pouches with indicated treatments. Split signals representing rearrangements are highlighted by arrows. The FISH images are accompanied by histograms representing the percentage of nuclei with split signals in TMPRSS2 and ERG. For each treatment, 100 nuclei were analyzed (*$p < 0.05$ by two-tailed Student's t test; error bars, SEM of two technical replicates).

(D) F4/80 staining reveals depletion of macrophages in mouse air pouches upon treatment with Clodrosome. Scale bar indicates 5 μm.

(E) Clodrosome treatment resulted in a reduction in total cellular infiltrate in air pouches (*$p < 0.01$ by two-tailed Student's t test; error bars, SEM of three mice).

(F) TaqMan qRT-PCR assays determine the *TMPRSS2-ERG* transcript level in LNCaP cells derived from LPS-stimulated (100 μg) C57BL/6 mouse air pouches with Encapsome or Clodrosome treatments (*$p < 0.01$ by two-tailed Mann-Whitney U-test). Each data point represents the mean of three technical replicates from an independent treatment.

(G) TaqMan qRT-PCR assays to determine *TMPRSS2-ERG* transcript level in LNCaP cells derived from LPS-stimulated (100 μg) C57BL/6 mouse air pouches with vehicle or JQ1 (100 mg/kg) treatments (*$p < 0.05$ by two-tailed Mann-Whitney U-test). Each data point represents the mean of three technical replicates from an independent treatment.

See also Figure S7.

is generated by the injection of sterile air under the dorsal skin of mice. Injection of an inflammatory irritant (e.g., lipopolysaccharides [LPS]) into the air pouch produces an inflammatory response that is characterized by the infiltration of inflammatory cells and the production of cytokines or chemokines (Romano et al., 1997). We injected 10 million LNCaP cells in control or LPS-treated air pouches raised in the immunodeficient severe combined immunodeficiency (SCID) mice or immunocompetent C57BL/6 mice (Figure 6A). The cells were recovered 24 hr post-injection by air-pouch lavage. We did not observe *TMPRSS2-ERG* gene fusion transcripts in LNCaP cells recovered from the air pouches of SCID mice with or without LPS treatment. By

contrast, *TMPRSS2-ERG* gene fusions were observed in LNCaP cells injected into the air pouch of C57BL/6 mice, the levels of which were further accentuated upon treatment with LPS (Figure 6B). These results suggest that analogous to our in vitro data, inflammation in vivo induces the formation of *TMPRSS2-ERG* gene fusions. We next optimized the split-signal-based dual-color FISH assay with *TMPRSS2* and *ERG* probes on LNCaP cells derived from the murine air pouch. These probes are human specific and do not cross-react with mouse cells (Figure S7B). Split-signal dual-color FISH assays revealed breaks in the *TMPRSS2* and *ERG* locus of LNCaP cells derived from C57BL/6 mice, but not SCID mice (Figures 6C and S7C). Because LPS was injected in the air pouch 1 day before cell implantation, a direct effect of LPS on LNCaP cells can be ruled out. Furthermore, because LPS-treated air pouches in the SCID mouse background did not induce the formation of gene fusions, we conclude that the observed effects are a consequence of host inflammation. In concordance with our previous results using TNF-α and gamma irradiation, the frequencies of inflammation-induced in vivo breaks were higher at the *TMPRSS2* locus compared to the *ERG* locus. This suggests that DNA breaks in *ERG* are a rate-limiting step in the formation of *TMPRSS2-ERG* gene fusions. Because the air pouch is a model of tissue injury, and human LNCaP cells are recognized as a foreign graft in C57BL/6 mice, there is substantial inflammation that adversely affects cell viability, given that the cells stay in the pouch for 24 hr.

Due to the emerging role of macrophages in tumor development (Qian and Pollard, 2010), we tested their role in LPS-mediated *TMPRSS2-ERG* gene fusion formation in the C57BL/6 mouse air-pouch model. We employed a liposome-based approach to deplete phagocytic cells (macrophages or neutrophils) from C57BL/6 mouse air pouches by injecting Clodrosome (in which clodronate is encapsulated in the aqueous compartment of the liposomes) or Encapsome, the vehicle control (Van Rooijen and Sanders, 1994; Zeisberger et al., 2006). The liposomes are not taken up by non-phagocytic cells; unencapsulated clodronate cannot cross the cell membrane to initiate cell death. Macrophage depletion was evaluated by immunofluorescence using the F4/80 monoclonal antibody that recognizes a macrophage-restricted cell surface glycoprotein (Figure 6D). Macrophage depletion resulted in a reduction in the total cellular infiltrate in the air pouch, suggesting impaired recruitment of other immune cells to the air pouch (Figure 6E).

We measured *TMPRSS2-ERG* gene fusion formation in LNCaP cells injected into LPS-stimulated C57BL/6 mouse air pouches with Encapsome treatment and compared this against treatment with Clodrosome (macrophage-depleted setting). While the Encapsome-treated group exhibited robust formation of *TMPRSS2-ERG* gene fusion, the effect was blocked in the Clodrosome-treated group (Figure 6F). These data clearly indicate a role for macrophages or neutrophils in *TMPRSS2-ERG* gene fusion formation. Because SCID mice contain macrophages, we conclude that macrophages are necessary, but not sufficient, for in vivo gene fusion formation. Our data suggest that a complex network of interactions between macrophages and other immune cell types (B and T cells) mediate gene fusion formation. Reports indicate a role for bromodomain and extraterminal domain (BET) protein inhibitors like JQ1 and I-BET in suppressing inflammation (Belkina et al., 2013; Nicodeme et al., 2010). BET inhibition has been shown to decrease proinflammatory cytokine production in macrophages and ablate inflammatory responses in mouse models. We observe that treatment with JQ1 blocks *TMPRSS2-ERG* gene fusion formation in the air-pouch model for in vivo inflammation (Figure 6G). Because JQ1 also blocks AR function (Asangani et al., 2014), it is conceivable that the observed effects are due to a combined suppression of inflammation and androgen signaling. We thereby present definitive evidence for the role of inflammation in gene fusion formation.

DISCUSSION

Altogether, these results implicate a critical role for inflammation-induced oxidative stress in the formation of DNA breaks leading to recurrent gene rearrangements in prostate cancer. Although other potential mechanisms of DNA breaks exist, we suspect that inflammation-induced oxidative stress may be a significant contributor of DNA damage. Endonucleases like RAG and AID have been implicated the formation of DNA breaks, resulting in genomic rearrangements involving the immunoglobulin loci. For example, the RAG complex and AID are involved in the formation of the follicular lymphoma-associated t(14;18) *BCL2-IGH* translocation and Burkitt's lymphoma-associated t(8;14) IGH-MYC translocations, respectively (Ramiro et al., 2004; Tsujimoto et al., 1985). Because the expression levels of these endonucleases are very low or undetectable in the normal prostate or prostate cancers, these are unlikely to be physiologically relevant in the genesis of prostate cancer-associated genomic rearrangements. Although transcription can introduce breaks in 5′ gene fusion partners that are highly expressed (e.g., *TMPRSS2*), most 3′ partners such as *ERG* and *ETV1* exhibit no or minimal transcription in the prostate gland before gene fusion formation (Haffner et al., 2010). Thus, transcription alone cannot explain the formation of DNA breaks in both partner genes leading to ETS gene fusions. Genotoxic drugs (e.g., clastogens), chemotherapeutic drugs (e.g., cisplatin), topoisomerase inhibitors (e.g., camptothecin and etoposide), and other drugs such as hydroxyurea and aphidicolin can induce DNA double-strand breaks. ETS gene fusions are early events and arise in patients before they are treated with any of these drugs. Thus, exposure to such drugs may not contribute to DNA breaks leading to ETS gene fusions in prostate cancer. While DNA replication is considered a major source of DNA breaks, the prostate luminal cells, which are widely believed to be the cell of origin for prostate cancer, are post-mitotic cells. Neuroendocrine cells in the prostate lumen are also post-mitotic. The basal cells of the prostate have a very low mitotic index. Thus, cell division or DNA replication is not likely to be a major contributor to DNA breaks required for ETS gene fusion formation in the prostate. Although ionizing radiation is an excellent external source of DNA damage, the in vivo sources of DNA breaks that contribute to the formation of genomic rearrangements in prostate cancer are not well defined.

We suggest that inflammation-induced oxidative stress is a major source of DNA breaks in the human prostate. The

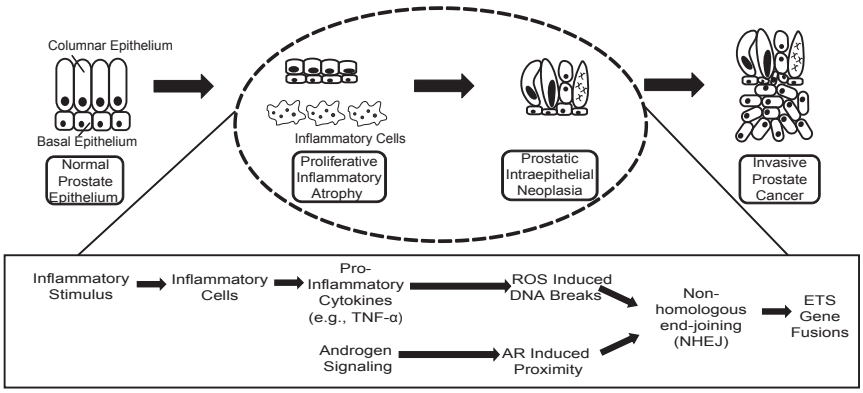

Figure 7. Proposed Model for Inflammation-Induced Gene Fusion Formation in Prostate Cancer

Proliferative inflammatory atrophy (PIA) is associated with inflammatory cells that secrete pro-inflammatory cytokines (e.g., TNF-α). This results in the formation of ROS-induced DNA breaks, which in combination with androgen signaling-induced proximity between gene fusion partner loci, can facilitate ETS gene fusion formation, thereby promoting prostate cancer development.

upstream triggers for inflammation can be diet, lifestyle, infection, and even the normal process of aging. While the potential association between inflammation and prostate cancer is not new, there are few direct mechanistic links of inflammation to recurrent driver mutations in cancer. By building on earlier work on chromosomal proximity and DNA rearrangements (Baca et al., 2013; Berger et al., 2011), our working model suggests that AR induces the proximity of genes such as *TMPRSS2* and *ERG* (Lin et al., 2009; Mani et al., 2009), while inflammatory stimuli trigger DNA breaks via oxidative stress (Figure 7). Our studies implicate microhomology-mediated NHEJ as the repair process contributing to inflammation-induced de novo genomic rearrangements. The strong association of PIA with human prostate cancer may represent circumstantial morphologic evidence for this link (De Marzo et al., 1999). These studies suggest that anti-inflammatories may have a role in the chemoprevention of prostate cancer, as suggested by published epidemiological studies (De Marzo et al., 2007; Nelson et al., 2003; Sfanos and De Marzo, 2012). Broadly, while these studies have been carried out in a prostate cancer model, the results suggest a potential role for inflammation-induced oxidative stress in the genesis of gene fusions across different cancer types.

EXPERIMENTAL PROCEDURES

Cell Culture, Transfection, Immunofluorescence, and Immunoblot Analysis

LNCaP and DU145 cells were cultured in RPMI 1640 medium containing 10% fetal bovine serum (FBS) in a 5% CO_2 humidified incubator. LAPC-4 and VCaP cells were cultured in Iscove's modified Dulbecco's medium (IMDM) and DMEM, respectively, supplemented with 10% FBS.

For in vitro stimulation experiments, cells were treated with 100 ng/mL TNF-α (Sigma) for various time intervals. For androgen depletion experiments, the cells were cultured in phenol-red free media containing 10% charcoal-stripped serum (HyClone) for 2 days.

Non-targeting siRNA (D-001810-10), AR siRNA (J-003400-08), ataxia telangiectasia mutated (ATM) siRNA (L-003201-00-0050), BRCA1 siRNA (L-003461-00-0050), and RAD51 siRNA (L-003530-00-0050) were obtained from Dharmacon. siRNA was transfected using Lipofectamine RNAiMAX transfection reagent (Invitrogen, #13778-150) according to the manufacturer's protocol.

For immunofluorescence analysis, cells were fixed in ice-cold methanol, followed by blocking, incubation with primary antibodies against RAD51 (Santa Cruz Biotechnology, #sc-8349), and detection with anti-rabbit secondary antibodies conjugated to Alexa Fluor 594 (Thermo Fisher Scientific, #A-21207). Images were captured by confocal microscopy (Zeiss, #LSM 880). The staining intensity was analyzed using the CellProfiler software (Carpenter et al., 2006). For immunoblot analysis, mouse monoclonal antibodies against phosphorylated histone H2A.X (Ser139) (Millipore, #05-636), rabbit monoclonal antibodies against ERG (Epitomics, #2805-1), and rabbit polyclonal antibodies against androgen receptor (Millipore, #06-680), histone H2A.X (Cell Signaling Technology, #2595S), and β-tubulin (Santa Cruz Biotechnology, #sc-9104) were used.

Gene Expression Studies

qRT-PCR was performed using Power SYBR Green PCR master mix (Applied Biosystems) or TaqMan Universal PCR master mix (Applied Biosystems) on a 7900HT Fast Real-Time PCR system (Applied Biosystems), as described previously (Laxman et al., 2006; Mani et al., 2009; Tomlins et al., 2005). To synthesize cDNA, 3 μg of total RNA was used. In each RT-PCR analysis, 3% of the cDNA representing 90 ng of the original RNA was used. Primers for SYBR green assays for *GAPDH* and *ERG* (exons 5 and 6) were as described (Tomlins et al., 2005). TaqMan gene expression assay for *GAPDH* was obtained from Applied Biosystems (Assay ID: Hs00266705_g1). Primers and the minor groove binder (MGB) probe for *TMPRSS2-ERG* (TaqMan assay) are TM_ERGa-3-f: 5′-CTGGAGCGCGGCAGGAA-3′; TM_ERGa-3-r: 5′-CCGTAGGCACACTCAAACAACGA-3′; and TM_ERGa-3-probe: 5′-TTATCAGTTGTGAGTGAGGAC-3′. SYBR green *GAPDH* assay was used for all in vitro studies; TaqMan *GAPDH* that is human specific was used for all mouse air-pouch studies. Primers for *TMPRSS2-ERG* gel-based nested RT-PCR (Figures 1A and 6B) are 1For: 5′-CAGGAGGCGGAGGCGGA-3′; 1Rev: 5′-GGCGTTGTAGCTGGGGGTGAG-3′; 2For: 5′-AGCGCGGCAGGTTATTCCA-3′; and 2Rev: 5′-ATCATGTCCTTCAGTAAGCCA-3′. The *TMPRSS2-ERG* TaqMan assay in LAPC-4 and DU145 cells (Figure 1E) was preceded by 15-cycle preamplification using the 1For and 1Rev primers, as described earlier. qRT-PCR primers for *ATM* (#PPH00325C-200), *BRCA1* (#PPH00322F-200), and *RAD51* (#PPH00942F-200) were obtained from SABiosciences. Primers for *TMPRSS2-ETV1* gel-based nested RT-PCR (Figure 5E), *TMPRSS2-ETV1* qRT-PCR, *ACTIN* gel-based RT-PCR, and *BCR-ABL1* gel-based RT-PCR and qRT-PCR are described elsewhere (Lin et al., 2009).

ROS Assay

Intracellular ROS was detected by fluorescence-activated cell sorting (FACS) analysis of ~60,000 LNCaP cells with various treatments using the Total Reactive Oxygen Species (ROS) Assay Kit 520 nm (eBioscience) according to the manufacturer's protocol.

ACCESSION NUMBERS

The accession number for the custom capture sequence data used to detect genomic breakpoints and reported in this paper (Figures 2D and S3) is NCBI SRA: SRP090763.

SUPPLEMENTAL INFORMATION

Supplemental Information includes Supplemental Experimental Procedures and seven figures and can be found with this article online at http://dx.doi.org/10.1016/j.celrep.2016.11.019.

AUTHOR CONTRIBUTIONS

Conception and design: R.S.M. and A.M.C.; Development of methodology: R.S.M., S.R., N.P., H.A.S., P.K., A.E.K., and A.M.C.; Acquisition of data: R.S.M., M.A.A., X.L., L.W., A.G., A.A., S.G.R., B.J.R., W.K., M.T., X.C., S.M.D., and N.P.; Analysis and interpretation of data: R.S.M., X.L., S.K.-S., B.A.V., N.P., and A.M.C.; Writing, review, and/or revision of the manuscript: R.S.M. and A.M.C.; Study supervision: R.S.M. and A.M.C.

ACKNOWLEDGMENTS

We thank D. Robinson, Y. Wu, and J. Pan for assistance with custom capture sequencing and S. Carskadon for technical assistance. NIH Pathway to Independence (PI) Award R00CA160640 to R.S.M. and startup funds from UT Southwestern supported research reported in this publication. R.S.M. also acknowledges funding from the ACS-IRG New Investigator Award in Cancer Research (IRG-02-196) and the Stewart Rahr-Prostate Cancer Foundation Young Investigator Award. This work was supported in part by NIH Prostate SPORE (P50CA186786), the Early Detection Research Network (U01 CA111275 and R01CA132874), and the Prostate Cancer Foundation. A.M.C. is an American Cancer Society research professor and an A. Alfred Taubman scholar.

A.M.C. is a co-inventor on a patent filed by the University of Michigan covering the diagnostic and therapeutic field of use for ETS fusions in prostate cancer. The diagnostic field of use has been licensed to Hologic. Hologic did not play a role in the design and conduct of this study; in the collection, analysis, or interpretation of the data; or in the preparation, review, or approval of the article.

Received: June 10, 2016
Revised: September 9, 2016
Accepted: November 2, 2016
Published: December 6, 2016

REFERENCES

Asangani, I.A., Dommeti, V.L., Wang, X., Malik, R., Cieslik, M., Yang, R., Escara-Wilke, J., Wilder-Romans, K., Dhanireddy, S., Engelke, C., et al. (2014). Therapeutic targeting of BET bromodomain proteins in castration-resistant prostate cancer. Nature *510*, 278–282.

Baca, S.C., Prandi, D., Lawrence, M.S., Mosquera, J.M., Romanel, A., Drier, Y., Park, K., Kitabayashi, N., MacDonald, T.Y., Ghandi, M., et al. (2013). Punctuated evolution of prostate cancer genomes. Cell *153*, 666–677.

Balkwill, F., and Mantovani, A. (2001). Inflammation and cancer: back to Virchow? Lancet *357*, 539–545.

Baud, V., and Karin, M. (2001). Signal transduction by tumor necrosis factor and its relatives. Trends Cell Biol. *11*, 372–377.

Belkina, A.C., Nikolajczyk, B.S., and Denis, G.V. (2013). BET protein function is required for inflammation: Brd2 genetic disruption and BET inhibitor JQ1 impair mouse macrophage inflammatory responses. J. Immunol. *190*, 3670–3678.

Berger, M.F., Lawrence, M.S., Demichelis, F., Drier, Y., Cibulskis, K., Sivachenko, A.Y., Sboner, A., Esgueva, R., Pflueger, D., Sougnez, C., et al. (2011). The genomic complexity of primary human prostate cancer. Nature *470*, 214–220.

Blaser, H., Dostert, C., Mak, T.W., and Brenner, D. (2016). TNF and ROS crosstalk in inflammation. Trends Cell Biol. *26*, 249–261.

Carpenter, A.E., Jones, T.R., Lamprecht, M.R., Clarke, C., Kang, I.H., Friman, O., Guertin, D.A., Chang, J.H., Lindquist, R.A., Moffat, J., et al. (2006). CellProfiler: image analysis software for identifying and quantifying cell phenotypes. Genome Biol. *7*, R100.

Chandel, N.S., Schumacker, P.T., and Arch, R.H. (2001). Reactive oxygen species are downstream products of TRAF-mediated signal transduction. J. Biol. Chem. *276*, 42728–42736.

Consortium, E.P., Bernstein, B.E., Birney, E., Dunham, I., Green, E.D., Gunter, C., and Snyder, M.; ENCODE Project Consortium (2012). An integrated encyclopedia of DNA elements in the human genome. Nature *489*, 57–74.

Coussens, L.M., and Werb, Z. (2002). Inflammation and cancer. Nature *420*, 860–867.

De Marzo, A.M., Marchi, V.L., Epstein, J.I., and Nelson, W.G. (1999). Proliferative inflammatory atrophy of the prostate: implications for prostatic carcinogenesis. Am. J. Pathol. *155*, 1985–1992.

De Marzo, A.M., Platz, E.A., Sutcliffe, S., Xu, J., Grönberg, H., Drake, C.G., Nakai, Y., Isaacs, W.B., and Nelson, W.G. (2007). Inflammation in prostate carcinogenesis. Nat. Rev. Cancer *7*, 256–269.

Edwards, J.C., Sedgwick, A.D., and Willoughby, D.A. (1981). The formation of a structure with the features of synovial lining by subcutaneous injection of air: an in vivo tissue culture system. J. Pathol. *134*, 147–156.

Grivennikov, S.I., Greten, F.R., and Karin, M. (2010). Immunity, inflammation, and cancer. Cell *140*, 883–899.

Haffner, M.C., Aryee, M.J., Toubaji, A., Esopi, D.M., Albadine, R., Gurel, B., Isaacs, W.B., Bova, G.S., Liu, W., Xu, J., et al. (2010). Androgen-induced TOP2B-mediated double-strand breaks and prostate cancer gene rearrangements. Nat Genet. *42*, 668–675.

Kim, J.J., Lee, S.B., Park, J.K., and Yoo, Y.D. (2010). TNF-alpha-induced ROS production triggering apoptosis is directly linked to Romo1 and Bcl-X(L). Cell Death Differ. *17*, 1420–1434.

Kim, Y.S., Morgan, M.J., Choksi, S., and Liu, Z.G. (2007). TNF-induced activation of the Nox1 NADPH oxidase and its role in the induction of necrotic cell death. Mol. Cell *26*, 675–687.

Laxman, B., Tomlins, S.A., Mehra, R., Morris, D.S., Wang, L., Helgeson, B.E., Shah, R.B., Rubin, M.A., Wei, J.T., and Chinnaiyan, A.M. (2006). Noninvasive detection of TMPRSS2:ERG fusion transcripts in the urine of men with prostate cancer. Neoplasia *8*, 885–888.

Lin, C., Yang, L., Tanasa, B., Hutt, K., Ju, B.G., Ohgi, K., Zhang, J., Rose, D.W., Fu, X.D., Glass, C.K., and Rosenfeld, M.G. (2009). Nuclear receptor-induced chromosomal proximity and DNA breaks underlie specific translocations in cancer. Cell *139*, 1069–1083.

Maher, C.A., Kumar-Sinha, C., Cao, X., Kalyana-Sundaram, S., Han, B., Jing, X., Sam, L., Barrette, T., Palanisamy, N., and Chinnaiyan, A.M. (2009). Transcriptome sequencing to detect gene fusions in cancer. Nature *458*, 97–101.

Mani, R.S., Tomlins, S.A., Callahan, K., Ghosh, A., Nyati, M.K., Varambally, S., Palanisamy, N., and Chinnaiyan, A.M. (2009). Induced chromosomal proximity and gene fusions in prostate cancer. Science *326*, 1230.

Moynahan, M.E., and Jasin, M. (2010). Mitotic homologous recombination maintains genomic stability and suppresses tumorigenesis. Nat. Rev. Mol. Cell Biol. *11*, 196–207.

Nelson, W.G., De Marzo, A.M., and Isaacs, W.B. (2003). Prostate cancer. N. Engl. J. Med. *349*, 366–381.

Nicodeme, E., Jeffrey, K.L., Schaefer, U., Beinke, S., Dewell, S., Chung, C.W., Chandwani, R., Marazzi, I., Wilson, P., Coste, H., et al. (2010). Suppression of inflammation by a synthetic histone mimic. Nature *468*, 1119–1123.

Qian, B.Z., and Pollard, J.W. (2010). Macrophage diversity enhances tumor progression and metastasis. Cell *141*, 39–51.

Ramiro, A.R., Jankovic, M., Eisenreich, T., Difilippantonio, S., Chen-Kiang, S., Muramatsu, M., Honjo, T., Nussenzweig, A., and Nussenzweig, M.C. (2004). AID is required for c-myc/IgH chromosome translocations in vivo. Cell *118*, 431–438.

Romano, M., Faggioni, R., Sironi, M., Sacco, S., Echtenacher, B., Di Santo, E., Salmona, M., and Ghezzi, P. (1997). Carrageenan-induced acute inflammation

in the mouse air pouch synovial model. Role of tumour necrosis factor. Mediators Inflamm. *6*, 32–38.

Rowley, J.D. (1973). Letter: a new consistent chromosomal abnormality in chronic myelogenous leukaemia identified by quinacrine fluorescence and Giemsa staining. Nature *243*, 290–293.

Sfanos, K.S., and De Marzo, A.M. (2012). Prostate cancer and inflammation: the evidence. Histopathology *60*, 199–215.

Teles Alves, I., Hiltemann, S., Hartjes, T., van der Spek, P., Stubbs, A., Trapman, J., and Jenster, G. (2013). Gene fusions by chromothripsis of chromosome 5q in the VCaP prostate cancer cell line. Hum. Genet. *132*, 709–713.

Thurman, R.E., Rynes, E., Humbert, R., Vierstra, J., Maurano, M.T., Haugen, E., Sheffield, N.C., Stergachis, A.B., Wang, H., Vernot, B., et al. (2012). The accessible chromatin landscape of the human genome. Nature *489*, 75–82.

Tomlins, S.A., Rhodes, D.R., Perner, S., Dhanasekaran, S.M., Mehra, R., Sun, X.W., Varambally, S., Cao, X., Tchinda, J., Kuefer, R., et al. (2005). Recurrent fusion of TMPRSS2 and ETS transcription factor genes in prostate cancer. Science *310*, 644–648.

Tomlins, S.A., Laxman, B., Dhanasekaran, S.M., Helgeson, B.E., Cao, X., Morris, D.S., Menon, A., Jing, X., Cao, Q., Han, B., et al. (2007). Distinct classes of chromosomal rearrangements create oncogenic ETS gene fusions in prostate cancer. Nature *448*, 595–599.

Tsujimoto, Y., Gorham, J., Cossman, J., Jaffe, E., and Croce, C.M. (1985). The t(14;18) chromosome translocations involved in B-cell neoplasms result from mistakes in VDJ joining. Science *229*, 1390–1393.

Van Rooijen, N., and Sanders, A. (1994). Liposome mediated depletion of macrophages: mechanism of action, preparation of liposomes and applications. J. Immunol. Methods *174*, 83–93.

Weier, C., Haffner, M.C., Mosbruger, T., Esopi, D.M., Hicks, J., Zheng, Q., Fedor, H., Isaacs, W.B., De Marzo, A.M., Nelson, W.G., and Yegnasubramanian, S. (2013). Nucleotide resolution analysis of TMPRSS2 and ERG rearrangements in prostate cancer. J. Pathol. *230*, 174–183.

Yazdanpanah, B., Wiegmann, K., Tchikov, V., Krut, O., Pongratz, C., Schramm, M., Kleinridders, A., Wunderlich, T., Kashkar, H., Utermöhlen, O., et al. (2009). Riboflavin kinase couples TNF receptor 1 to NADPH oxidase. Nature *460*, 1159–1163.

Zeisberger, S.M., Odermatt, B., Marty, C., Zehnder-Fjällman, A.H., Ballmer-Hofer, K., and Schwendener, R.A. (2006). Clodronate-liposome-mediated depletion of tumour-associated macrophages: a new and highly effective anti-angiogenic therapy approach. Br. J. Cancer *95*, 272–281.